Physica B 480 (2016) 68–71

Contents lists available at ScienceDirect

Physica B

journal homepage: www.elsevier.com/locate/physb

Transport characteristics of *n*-ZnO/*p*-Si heterojunction as determined from temperature dependent current–voltage measurements

S.R. Tankio Djiokap *, Z.N. Urgessa, C.M. Mbulanga, A. Venter, J.R. Botha

Department of Physics, Nelson Mandela Metropolitan University, P.O. Box 77000, Port Elizabeth 6031, South Africa

ARTICLE INFO

Article history:
Received 18 May 2015
Received in revised form
5 August 2015
Accepted 7 August 2015
Available online 11 August 2015

Keywords:
ZnO
Chemical bath deposition
Current–voltage measurements
Transport mechanism
Tunneling

ABSTRACT

Zinc oxide (ZnO) nanorods have been synthesized by a two-step chemical bath deposition process on silicon substrates having different dopant densities and orientations. Scanning electron microscopy and X-ray diffraction analysis reveal that the orientation of the Si substrate does not affect the orientation, distribution or crystallinity of the nanostructures. The electrical properties of the ZnO/Si heterojunction are also investigated by current–voltage (*I–V*) measurements. The ideality factor is found to be 2.6 at 295 K, indicating that complex current transport mechanisms are at play. Temperature dependent *I–V* characteristics have been used to determine the dominant transport mechanism. The experimental results suggest that in the low bias region the current is dominated by a trap assisted multi-step tunneling process.

1. Introduction

Zinc oxide (ZnO), a wide band gap semiconductor, is attracting much attention because of its potential for novel ultraviolet (UV) opto-electronic nanostructures. ZnO exhibits a large exciton binding energy (60 meV), allowing for exciton-governed UV light emission at room temperature [1]. In addition, ZnO-based materials are used for various applications such as solar cells [2], piezoelectric transducers [3], chemical sensors [4] and UV detectors [5]. Furthermore, ZnO nanostructures, such as nanorods (NRs) [6], nanowires [7] and nanotubes [8], have been widely investigated in the past several years due to their superior electrical and optical properties compared to planar structures. However, light emission from ZnO homojunctions is as yet difficult to achieve due to the lack of stable and/or reproducible *p*-type doping of ZnO. This difficulty has prompted researchers to also focus on *p–n* heterojunctions using various different substrates. Silicon (Si) has been a substrate of choice as it is cheap and readily available. Thus, diode-like rectifying junctions of ZnO NRs on Si substrates have been grown using a chemical bath deposition technique. This technique is reasonably simple and ZnO is cheap to produce [9]. The transport mechanisms of this junction are at present, however, not well understood.

In this study, the current transport mechanisms of ZnO/Si heterojunctions are investigated. The heterojunctions were fabricated by growing ZnO nanorods on Si (100) and (111) substrates using chemical bath deposition. The morphological and structural characteristics of the nanorod films were studied by scanning electron microscopy (SEM) and X-ray diffraction (XRD), while the electrical properties of the ZnO/Si junction were characterized by temperature dependent dark current–voltage (*I–V*) measurements.

2. Experiment

The Si wafers used in this study were bought from Virginia Semiconductor, whereas the chemicals for nanorod synthesis were purchased from Sigma Aldrich and were used without any additional purification. A two-step chemical bath deposition technique, described in detail elsewhere, was used to grow the nanorods [10]. The first step involved the formation of a seed layer, using an ethanolic solution of zinc acetate, producing ZnO nanoparticles that act as nucleation sites on the substrate. This was followed by the growth of ZnO nanorods from solution, using a mixture of aqueous solutions of zinc nitrate hexahydrate and hexamine. The morphology of the nanostructures was investigated by a field emission scanning electron microscope (JEOL 7001F FE-SEM), while the crystallinity was determined using a Bruker D8 Discover X-ray diffractometer (XRD) employing a Cu K_α X-ray source with a wavelength of 0.154 nm. Following a standard cleaning procedure as described in [10], circular aluminum ohmic contacts, 0.5 mm in diameter and 100 nm thick were resistively evaporated onto the ZnO surface. No annealing was required. Ohmic contact to the *p*-Si surface was established using InGa eutectic. Prior to performing *I–V* measurements on the heterostructures, the individual

* Corresponding author.
E-mail address: stive.tankiodjiokap@nmmu.ac.za (S.R.T. Djiokap).

http://dx.doi.org/10.1016/j.physb.2015.08.013
0921-4526/

constituents of the heterostructures were metalized and assessed independently (i.e. Al/*p*-Si/InGa and Al/*n*-ZnO/Al). The *I*–*V* characteristics of the grown *n*-ZnO/*p*-Si heterostructures were obtained by using a programmable integrated HP4140B pA meter/DC voltage source. Both constituents displayed ohmic behavior suggesting that the observed rectification is a consequence of junction formation between the *n*-ZnO rods and the *p*-Si substrate.

3. Results and discussion

Si wafers with different orientations and dopant densities were used for the growth of the ZnO/Si heterojunctions. In the discussion that follows, A and B refer to heterojunctions for which Si (100) with carrier concentrations of ~1×10^{18} cm^{-3} and ~1×10^{16} cm^{-3}, respectively, were used. For heterojunction C, the ZnO nanorods were grown on Si (111) with a carrier concentration of ~1×10^{17} cm^{-3}.

Fig. 1(a) and (b) depicts top view SEM micrographs of the ZnO nanorods for structures B and C, respectively. Evidently, the ZnO deposits are rod-like with hexagonal cross-sections. The average rod diameter, estimated from the SEM micrographs, is ~70 nm. Moreover, the insets in Fig. 1(a) and (b) of the cross-sectional view of the ZnO NRs show that the majority of the rods are perpendicular to the substrate surface. Fig. 1(c) displays a normalized XRD spectrum for structures B and C. Irrespective of the Si orientation the (0002) peak of ZnO is found to be the most dominant, indicating that the rods are preferentially orientated with the *c*-axis perpendicular to the substrate. This is consistent with the morphology observed in the cross-sectional SEM micrographs. The full-widths at half-maxima (FWHM) of the (0002) peaks for structures B and C are 0.324° and 0.329°, respectively, which are smaller compared to ZnO grown by vapor phase techniques [11,12], indicating a better crystallinity. The above results indicate that the planar orientation of the Si substrate does not affect the orientation, distribution or crystallinity of the grown nanorods. It has previously been reported that the mechanism for nucleation, which is controlled by the seed layer, is a crucial step in controlling the orientation and distribution of ZnO nanorods on silicon substrates [10]. In this study both substrates were seeded using similar experimental conditions. It is therefore reasonable to assume that the observed similarity in nanorod orientation and distribution is not related to the substrate orientation but rather to the structural properties (nucleation density etc.) of the seed layer.

Fig. 1(d) shows typical room temperature *I*–*V* characteristics of the ZnO/Si heterojunctions. Evidently the *I*–*V* characteristics depend on the carrier concentration with heterojunction A exhibiting ohmic behavior. This is attributed to the tunneling of carriers across the narrow depletion region ($W \propto (N_{D,A})^{-1/2}$). Additionally, the symmetry in the *I*–*V* curve (around 0 V) suggests that the nanorods are also heavily doped. It is also instructive to note that hydrogen, always present in these ZnO nanostructures, has been identified as a shallow donor and is most likely responsible for the large free carrier concentration at room temperature [13]. The *I*–*V* characteristics of heterojunction B, however, displays substantial rectification with a rectification ratio of ~19 measured at ±0.5 V. Structure C also displays rectifying behavior, with a rectification ratio of 8. The *I*–*V* characteristics are described by the following equation based on the conventional *p*–*n* heterojunction theory [14]

$$I = I_s \exp\left(\frac{qV}{nkT}\right), \tag{1}$$

where q is the electronic charge, n the ideality factor, k is the Boltzmann's constant, T the absolute temperature and I_s the reverse saturation current. The ideality factor, n, is determined from the slope of the log (I) vs V plot and is given by [15]

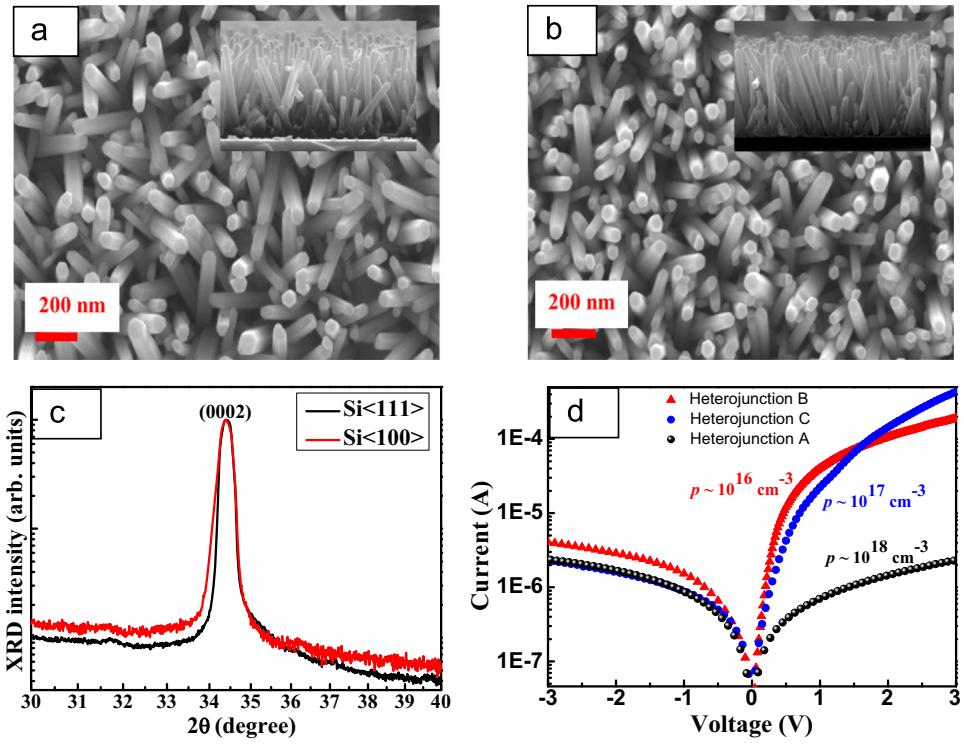

Fig. 1. (a,b) SEM micrographs (top views) of ZnO nanorods grown on Si (100) and Si (111), respectively. The insets are the corresponding cross-sectional images of the nanorods. (c) Normalized XRD spectra of ZnO nanorods grown on Si (100) and Si (111) respectively. (d) Room temperature *I*–*V* characteristics of ZnO/Si heterojunctions A, B and C.

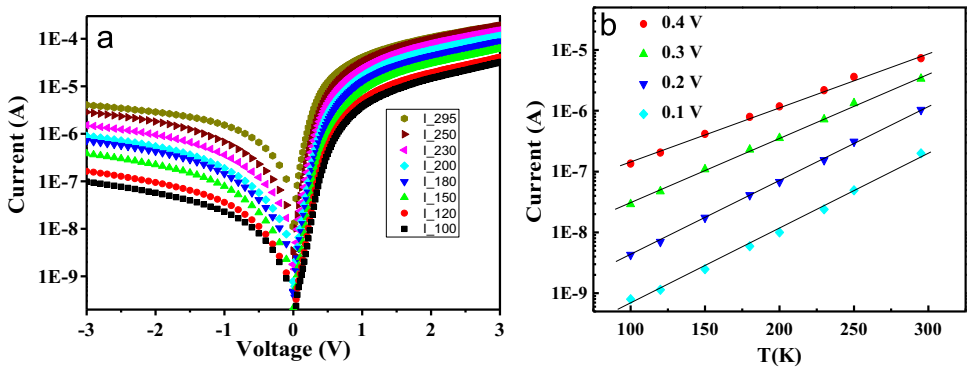

Fig. 2. (a) Temperature-dependent *I–V* characteristics of the ZnO/Si heterojunction (sample B). (b) Current as function of temperature at predetermined forward biases.

$$n = \frac{q}{kT}\left(\frac{dV}{d\left(\ln\left(I/I_s\right)\right)}\right). \tag{2}$$

Using Eq. (2), the room temperature ideality factors were found to be 2.6 and 4.96 for structures B and C respectively. For both these devices the ideality factor is significantly larger than 2, suggesting a complex current transport mechanism.

In order to establish the dominant carrier transport mechanism, temperature dependent *I–V* measurements were performed in the temperature range 100–295 K, for sample B ($N_A \sim 1 \times 10^{16}$ cm^{-3}. Fig. 2(a) shows the plot of log(I) versus V for this sample. Rectification is observed throughout this temperature range. The reverse current increases with increasing temperature due to an increase in the thermally generated minority carriers.

Fig. 2(b) shows the current response of the heterojunction as function of temperature ranging between 100 K and 295 K for various predetermined forward biases. From this information, by employing Eq. (1), the ideality factor and reverse saturation current for this device were extracted. The ideality factor decreases from 7.67 at 100 K to 2.6 at 295 K. The reverse saturation current (I_s) increases with increasing temperature. These diode parameters are listed in Table 1.

Similar non-ideal behavior has been observed by Zhang et al. in sol–gel produced ZnO/Si heterojunctions [16] and in chemically deposited Cu_2O/Si heterojunctions by Serin et al. [17]. In both these cases a linear dependence was observed for the log I vs T. Fig. 2(b) shows the temperature dependence of log I at constant predetermined forward biases. These voltages were selected from the rectifying region of the heterojunction for which the log I vs V curve was linear. Evidently a graph of log I vs T is linear throughout the temperature range for all the forward biases considered. Linear fitting of these curves produced slope values of 0.012 T^{-1} and 0.008 T^{-1} at 0.1 V and 0.4 V respectively. Similar *I–T* characteristics were used by Zhang et.al [16] and Serin et.al [17] to identify the current transport. These authors used a modified thermionic emission model to describe the current transport in their devices. This model is quantified by

$$I(V, T) = I_s(T)\exp(B(T)V), \tag{3}$$

where the parameter B is related to the slope of the ln I vs V.

The dominant transport mechanism can be determined by studying the temperature dependence of this parameter [16–21]. If parameter B is temperature dependent, the dominant transport mechanism is either diffusion in the case of $n = 1$ or recombination when $1 < n \leq 2$. If parameter B is constant, tunneling is considered to be the dominant transport mechanism.

Fig. 3(a) depicts the temperature dependence of the slope of the log$I$ vs V plot. Evidently parameter B (~15.1 V^{-1}) is independent of temperature, suggesting that tunneling is possibly the dominant transport mechanism in the bias region employed. The observed temperature independent *I–V* characteristics are consequently explained in terms of a multistep-trap assisted tunneling process [21]. At low temperatures the carriers are trapped by defects present at the interface between the ZnO and the Si. As the temperature increases these defects ionize, making progressively more carriers available for conduction.

The temperature dependence of the reverse saturation current, I_s , can be expressed as:

$$I_S \propto \exp\left(-\frac{E_a}{kT}\right), \tag{4}$$

where E_a is the thermal activation energy. Fig. 3(b) shows an Arrhenius plot of the pre-exponential function log I_s vs 1000/T. The Arrhenius plot consists of two linear regions between 200 K to 295 K and 100 K to 180 K, with activation energies of 0.074 eV and 0.015 eV respectively. Results reported in literature show that this Arrhenius plot can have either a single [16–18] or double slope [19,22]. A single slope suggests that tunneling occurs via a single type of defect/impurity. Hence the activation energy does not change as a function of temperature. However, the double slope observed in this study, together with temperature independence of B, is an indication that tunneling via at least two types of defects are involved in the multi-step tunneling capture/emission processes [19]. At low temperature (100–180 K) the defect with activation energy of ~15 meV dominates the tunneling process, whereas for temperatures above 180 K the bulk of the current is generated through recombination via a deeper (74 meV) defect.

Table 1
Temperature dependent ideality factor and reverse saturation current for a ZnO/Si heterojunction (sample B).

T (K)	n	I_s (nA)
100	7.67	0.15
120	6.39	0.26
150	5.12	0.49
180	4.26	0.95
200	3.83	1.50
230	3.32	5.50
250	3.07	8.30
295	2.60	40.0

4. Conclusions

ZnO nanorods were uniformly grown on Si substrates with different dopant densities and orientations. The average diameter of the nanorods was determined from SEM to be ~70 nm. XRD revealed that the NRs are highly *c*-axis oriented and predominantly perpendicular to the substrate. The *I–V–T*

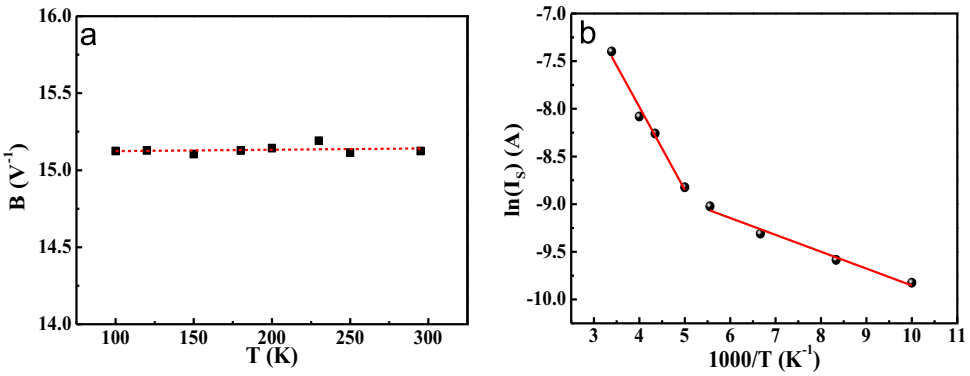

Fig. 3. (a) Temperature dependence of the parameter B in Eq. (3). (b) Arrhenius plot of $\log I_s$ vs $1000/T$.

characteristics, measured between 100 K and 295 K, suggest that multi-step, trap-assisted tunneling is the dominant transport mechanism in this temperature range and that at least two defects, with activations energy of 15 meV and 74 meV, are involved in this process.

Acknowledgments

This work is based upon research supported by the SA Research Chairs Initiative of the Department of Science and Technology and the National Research Foundation, South Africa. The financial support of the Nelson Mandela Metropolitan University is also gratefully acknowledged. William Goosen, Centre for High Resolution Transmission Electron Microscopy, NMMU, is acknowledged for the SEM micrographs. Thank you to SR Dobson, PhD student, NMMU, for proof reading.

References

[1] D.M. Bagnall, Y.F. Chen, Z. Zhu, T. Yao, S. Koyama, M.Y. Shen, T. Goto, Appl. Phys. Lett. 70 (1997) 2230.
[2] J.B. Baxter, E.S. Aydil, Appl. Phys. Lett. 86 (2005) 53114.
[3] T. Shiosaki, A. Kawabata, Appl. Phys. Lett. 25 (1974) 10.
[4] Q. Wan, Q.H. Li, Y.J. Chen, T.H. Wang, X.L. He, J.P. Li, C.L. Lin, Appl. Phys. Lett. 84 (2004) 3654.
[5] J.H. He, Y.H. Lin, M.E. McConney, V.V. Tsukruk, Z.L. Wang, G. Bao, J. Appl. Phys. 102 (2007) 084303.
[6] Y.-J. Lee, D.S. Ruby, D.W. Peters, B.B. McKenzie, J.W.P. Hsu, Nano Lett. 8 (2008) 1501.
[7] S.-W. Lee, M.-C. Jeong, J.-M. Myoung, G.-S. Chae, I.-J. Chung, Appl. Phys. Lett. 90 (2007) 133115.
[8] Y.J. Hong, H.S. Jung, J. Yoo, et al., Adv. Mater. 21 (2009) 222.
[9] Z.N. Urgessa, S.R. Dobson, K. Talla, D.M. Murape, A. Venter, J.R. Botha, Physica B 439 (2014) 149.
[10] Z.N. Urgessa, O.S. Oluwafemi, E.J. Olivier, J.H. Neethling, J.R. Botha, J. Alloy. Compd. 580 (2013) 120.
[11] J.B. You, X.W. Zhang, S.G. Zhang, H.R. Tan, J. Ying, Z.G. Yin, Q.S. Zhu, P.K. Chu, J. Appl. Phys. 107 (2010) 083701.
[12] Y.W. Zhang, X.M. Li, W.D. Yu, X.D. Gao, Y.F. Gu, C. Yang, J.L. Zhao, X.W. Sun, S. T. Tan, J.F. Kong, W.Z. Shen, J. Phys. D 41 (2008) 205105.
[13] Z.N. Urgessa, J.R. Botha, M.O. Eriksson, C.M. Mbulanga, S.R. Dobson, S.R. Tankio Djiokap, K.F. Karlsson, V. Khranovskyy, R. Yakimova, Per-Olof Holtz, J. Appl. Phys. 116 (2014) 123506.
[14] S.M. Sze, Physics of Semiconductor Devices, Second Edition, Wiley, New York, 1981.
[15] A. Gumus, A. Turut, N. Yalcin, J. Appl. Phys. 91 (2002) 245.
[16] Y. Zhang, J. Xu, B. Lin, Z. Fu, S. Zhong, C. Liu, Z. Zhang, Appl. Surf. Sci. 252 (2006) 3449.
[17] T. Serin, S. Gurakar, N. Serin, N. Yildirim, F. Ozyurt Kus, J. Phys. D: Appl. Phys. 42 (2009) 225108.
[18] J.D. Lee, C.Y. Park, H.S. Kim, J.J. Lee, Y.-G. Choo, J. Phys. D: Appl. Phys. 43 (2010) 365403.
[19] L.F. Marsal, I. Martin, J. Pallares, A. Orpella, R. Alcubilla, J. Appl. Phys. 94 (2003) 2622.
[20] D. Song, D.-H. Neuhaus, J. Xia, A.G. Aberle, Thin Solid Films 422 (2002) 180.
[21] A.R. Riben, D.L. Feucht, Int. J. Elektron. 20 (1966) 583.
[22] B.P. Modi, J.M. Dhimmar, IEEE 1627-4673, 978-1-4673-1627-9, 2012.